

Ultrafast Generation of Fundamental and Multiple-order Phonon Excitations in Highly-Enriched (6,5) Single-Wall Carbon Nanotubes

Y.-S. Lim,¹ A. R. T. Nugraha,² S.-J. Cho,¹ M.-Y. Noh,¹ E.-J. Yoon,³ H. Liu,⁴ J.-H. Kim,⁵ H. Telg,⁶ E. H. Háróz,⁶ G. D. Sanders,⁷ S.-H. Baik,⁸ H. Kataura,⁹ S. K. Doorn,⁶ C. J. Stanton,⁷ R. Saito,² J. Kono,^{5,10,11,*} and T. Joo^{3,†}

¹*Department of Nano Science and Mechanical Engineering and Nanotechnology Research Center, Konkuk University, Chungju, Chungbuk 380-701, Republic of Korea*

²*Department of Physics, Tohoku University, Sendai 980-8578, Japan*

³*Department of Chemistry, POSTECH, Pohang 790-784, Republic of Korea*

⁴*Beijing National Laboratory for Condensed Matter Physics,*

Institute of Physics, Chinese Academy of Sciences, Beijing 100190, China

⁵*Department of Electrical and Computer Engineering, Rice University, Houston, TX 77005, USA[‡]*

⁶*Center for Integrated Nanotechnologies, Los Alamos National Laboratory, Los Alamos, NM 87545, USA*

⁷*Department of Physics, University of Florida, Gainesville, FL 32611, USA*

⁸*Quantum Optics Research Division, Korea Atomic Energy Research Institute, Daejeon 305-353, Republic of Korea*

⁹*Nanosystem Research Institute, National Institute of Advanced Industrial Science and Technology, Tsukuba 305-8562, Japan*

¹⁰*Department of Physics and Astronomy, Rice University, Houston, TX 77005, USA*

¹¹*Department of Materials Science and NanoEngineering, Rice University, Houston, TX 77005, USA*

(Dated: July 2, 2021)

Using a macroscopic ensemble of highly-enriched (6,5) single-wall carbon nanotubes, combined with high signal-to-noise ratio, time-dependent differential transmission spectroscopy, we have generated vibrational modes in an ultrawide spectral range (10–3000 cm⁻¹). A total of fourteen modes were clearly resolved and identified, including fundamental modes of A, E₁, and E₂ symmetries and their combinational modes involving two and three phonons. Through comparison with CW Raman spectra as well as calculations based on an extended tight-binding model, we were able to identify all the observed peaks and determine the frequencies of the individual and combined modes. We provide a full summary of phonon frequencies for (6,5) nanotubes that can serve as a basic reference with which to refine our understanding of nanotube phonon spectra as well as a testbed for new theoretical models.

I. INTRODUCTION

Recent advances in separation and sorting techniques have allowed researchers to prepare highly-enriched, single-chirality macroscopic ensembles of single-wall carbon nanotubes (SWCNTs).^{1–8} This impressive progress is revolutionizing the field of carbon nanotube physics and chemistry, enabling detailed chirality-dependent spectroscopy studies that were previously impossible to perform.^{9–14} While many of the features in prior studies were obscured due to the many different chiralities present in the samples, in highly-enriched samples these features are better resolved, allowing one to study the intrinsic behaviors of one-dimensional (1-D) electrons, phonons, and excitons in SWCNTs in far greater detail. Moreover, the availability of highly-purified single-chirality SWCNTs opens up new possibilities for the development of optoelectronic devices^{15–19} that are useful for optical communications, spectroscopy, imaging, and sensing.

In this paper, we focus on the properties of phonons in SWCNTs generated through ultrafast optical excitation on a macroscopic ensemble of highly-enriched (6,5) SWCNTs.⁶ Raman spectroscopy has been an indispensable tool for characterizing and understanding the electronic and vibrational properties of graphite, SWCNTs, and graphene.^{20–25} Much accumulated knowledge exists on the strong Raman-active fundamental modes in SWC-

NTs such as the radial breathing mode (RBM), the D-mode, the G-mode, and the G' (or 2D) mode, observed through resonance Raman scattering spectroscopy. However, in contrast to graphite and graphene, SWCNTs are expected to exhibit many other fundamental modes arising from the large number of 1-D phonon branches that arise from circumferential quantization (or zone folding). At present, there is little experimental information available on these additional modes and their combinational modes, except some Raman studies of intermediate frequency modes (IFMs) in mixed-chirality samples.^{26–30} In addition to the problem that they are obscured in chirality-mixed samples, they are also difficult to detect because they couple weakly to the photo-excited carriers.

We utilized some of the advantages of coherent phonon (CP) spectroscopy³¹ to successfully observe and identify fourteen distinct phonon features in (6,5) SWCNTs. The two most important advantages of CP spectroscopy for the present study are its excellent frequency resolution (~ 0.4 cm⁻¹ in the current case) and the ease with which low-frequency modes can be observed due to the absence of the Rayleigh scattering or photoluminescence background. We have observed symmetry-allowed acoustic modes (with E₁ and E₂ symmetries) that are consistent with our calculations based on the extended tight-binding model. We also observed strong IFMs, which can be assigned to combinations between out-of-plane tangential optical (oTO) and acoustic phonons (E₁, E₂, and E₁+E₂

symmetries). Furthermore, we observed combinational modes between A symmetry optical phonons, that is, the RBM and the LO mode, and acoustic phonons (E_2 and E_1+E_2 symmetries). Finally, we provide a comprehensive list of phonon frequencies for (6,5) SWCNTs with assignments for both fundamental and combinational modes, based on a detailed comparison with our theoretical calculations of the full phonon dispersion curves for the (6,5) SWCNTs.

II. METHODS

Single-chirality (6,5) SWCNTs with 4 mM concentration were micelle suspended by 0.5 wt % DOC through the multicolumn gel chromatography isolation method.⁶

Pump-probe differential transmission measurements were performed on the solution in a quartz cell with an optical path length of 1 mm at room temperature. The light source for E_{11} excitation was a home-built Ti:Sapphire laser equipped with a double-chirped mirror set (DCM 7, Vteon, Inc.), which delivers pulses as short as 8 fs with a bandwidth over 400 nm centered around 800 nm. The probe beam was spectrally resolved by a set of bandpass filters with a bandwidth of 5 nm, prior to the photodetector. The intensity ratio between the pump and probe beams was $\sim 7/2$. Compared to frequency-domain Raman spectroscopy, time-domain CP spectroscopy has several advantages: a high frequency resolution, the absence of Rayleigh scattering background at low frequencies, no interference by photoluminescence, and an ability to directly measure vibration dynamics in the time domain. In a CP experiment, the high-frequency limit that can be detected depends on the pulse widths of the pump/probe beams; 10 fs pulses can generate and detect vibrational frequencies as high as 3000 cm^{-1} . Furthermore, time-resolved CP spectra can directly investigate not only the decay dynamics of each active phonon, such as anharmonic decay processes of optical phonons, but spectrally-resolved CP spectra also provide information on excited-state phononic levels, accessible for the third order optical process involved in the pump/probe scheme, and initial phase change of phonon oscillations related to the bandgap modulations induced by the radial breathing motion.^{31,32}

The phonon dispersions of the (6,5) SWCNT were obtained within an extended (long-range and symmetry-adapted) tight-binding model employing a specific force constant set.³³ This approach takes into account the curvature effects of the SWCNT in the calculation of the force constant parameters derived from the graphene force constants. The graphene force constant parameters were calculated by fitting the phonon dispersion from inelastic X-ray scattering experiment.³⁴

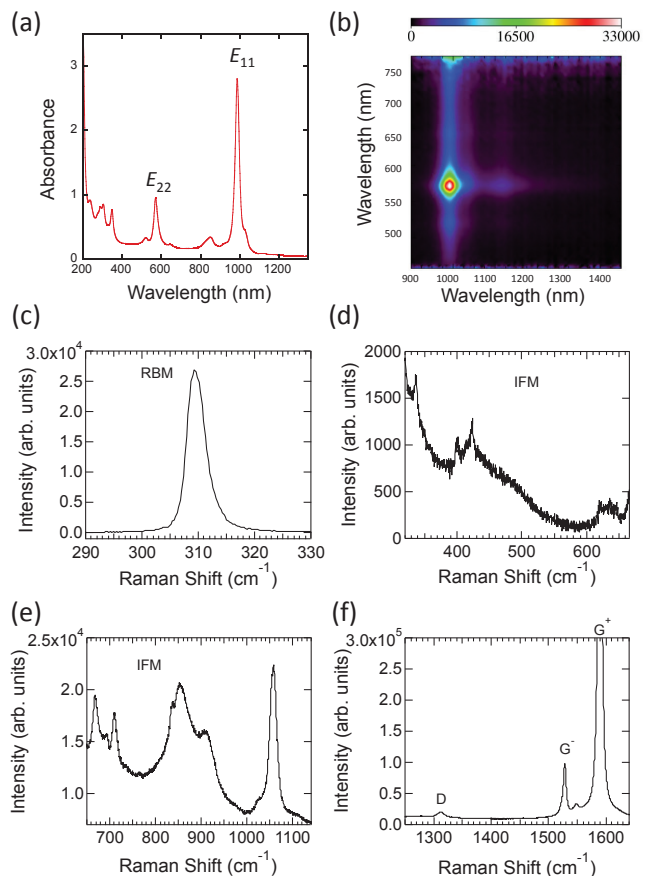


FIG. 1: (a) Absorption and (b) photoluminescence excitation spectra for the (6,5)-enriched SWCNT sample. (c)-(f) Continuous-wave Raman spectra taken with an excitation wavelength of 561.3 nm for different frequency ranges from 290 cm^{-1} to 1640 cm^{-1} . Although the vertical scales are given in arbitrary units, the relative scales are the same for (c)-(f).

III. RESULTS

Figure 1a shows the absorption spectrum in the near-infrared, visible, and ultraviolet for the highly-enriched (6,5) SWCNT sample. The largest absorption peaks are attributed to the lowest-energy interband resonances, E_{11} and E_{22} , which occur at 985 nm (1.26 eV) and 575 nm (2.16 eV), respectively. These values are in good agreement with those reported for other studies of (6,5) SWCNTs.¹⁹ The other smaller features are due to the phonon sidebands of the E_{11} and E_{22} peaks as well as higher-order (E_{33} , E_{44} , etc.) interband transitions in the shortest wavelength region of the spectrum. The narrow widths of the absorption lines attest to the high quality and purity of the (6,5) samples. Figure 1b shows a photoluminescence excitation map for the sample, plotting the excitation wavelength on the vertical axis versus emission wavelength on the horizontal axis. The strong spot observed at an excitation wavelength of

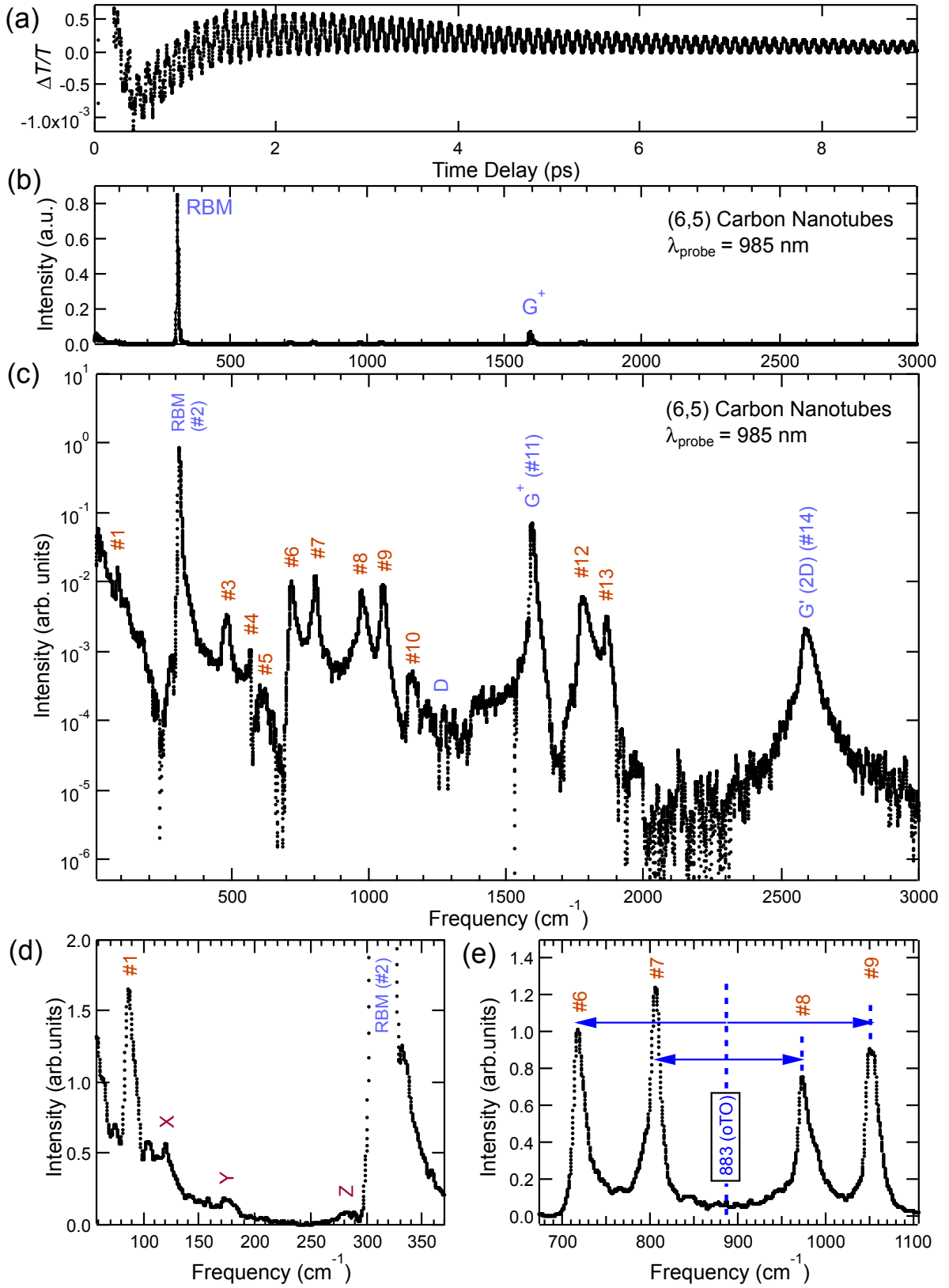


FIG. 2: (a) Differential transmission trace at a probe wavelength of 975 nm for (6,5) single-wall carbon nanotubes showing ultrafast oscillations due to coherent phonons. (b) and (c): Coherent phonon spectrum obtained through Fourier transformation of the data in (a) in linear and log scales, respectively, showing many phonon modes, labeled #1-#15. (d) The lowest frequency range, showing Peaks #1-#3, together with three less distinct peaks (X, Y, and Z). (e) Intermediate frequency modes, displaying symmetric pairs as sidebands of the oTO mode ($\sim 883 \text{ cm}^{-1}$).

575 nm and an emission wavelength of 985 nm is consistent with the E_{11} and E_{22} peaks in the absorption spectrum. No other spot is visible in the map, demonstrating the highly chirality-enriched nature of the sample. Figures 1c-f show continuous-wave (CW) Raman scattering spectra, taken *via* E_{22} resonance at an excitation wavelength of 561.3 nm, for different frequency ranges between 290 cm^{-1} and 1640 cm^{-1} . Although the vertical scales are given in arbitrary units, the relative scales are the same for Figs. 1c-f. In addition to the strong RBM (in c) and the D-mode and G-modes (in f), some weaker-intensity IFMs are observed (in d and e). The frequencies of these features are summarized in the fourth column of Table I.

Figure 2a shows a typical differential transmission trace in the time domain taken with ~ 8 fs pump pulses with a bandwidth over 400 nm centered around 800 nm together with a probe beam with a 5-nm bandwidth centered at 975 nm. The data exhibits ultrafast oscillations, containing various frequency components, the strongest of which are the RBM at $\sim 310\text{ cm}^{-1}$ and the G^+ (LO) mode at $\sim 1590\text{ cm}^{-1}$, as seen in the Fourier spectrum (Fig. 2b). Figure 2c shows the same spectrum as 2b but on a logarithmic scale in order to highlight a number of smaller-intensity modes. We can clearly identify fourteen distinct features, labeled #1-#14 in Fig. 2c, the highest-frequency mode being the G' (or 2D) mode at $\sim 2590\text{ cm}^{-1}$. An expanded view of the lowest-frequency region of the spectrum is given in Fig. 2d, showing Peak #1 at $\sim 85\text{ cm}^{-1}$ and Peak #2 (RBM) at $\sim 310\text{ cm}^{-1}$. In addition, there are three less distinct features at $\sim 120\text{ cm}^{-1}$, $\sim 180\text{ cm}^{-1}$, and $\sim 280\text{ cm}^{-1}$, which we label 'X', 'Y', and 'Z', respectively. Finally, the IFMs are shown in Fig. 2e, displaying the pair-wise appearance of six peaks above and below a central frequency of $\sim 883\text{ cm}^{-1}$. The frequencies of the observed fourteen peaks with estimated error bars are listed in the second column of Table I, together with their respective assignments in the third column, as discussed below.

IV. DISCUSSION

In a SWCNT, vibrational modes with A, E_1 , and E_2 symmetries are Raman active, and there are six modes in each symmetry.^{20-22,24} Among the phonon modes of the same order, the cutting line of the A mode is at the zone center of the graphene k -space while the cutting line of the E_1 (E_2) mode is the nearest (next nearest) to the zone center. Among the six A symmetry modes, the RBM, iTO, and LO are expected to have non-zero electron-phonon matrix elements at the Γ point ($q = 0$), and two acoustic phonon modes — the 'twiston' mode (TW) and the LA mode — are expected to have matrix elements at non-zero q . The E_1 and E_2 symmetry modes have weaker electron-phonon coupling than the A symmetry mode.³⁵ Figure 3a shows the phonon dispersion curves and the density of states for the (6,5) SWCNT calculated using

the extended tight-binding model.³⁵ It shows all possible E_1 , E_2 and E_n symmetries as well as A symmetry phonon branches. To investigate possible acoustic phonon modes at frequencies lower than the RBM, we enlarge the low frequency portion of the dispersion curve in Fig. 3b to display two branches for A and E_1 symmetry modes and one branch for the E_2 symmetry mode. In order to provide more insight into each mode, phonon dynamical matrix eigenvectors are shown in Fig. 3b, whose directions identify these modes as iTA-like or LA-like oscillations. In the last column of Table 1, we list the $q = 0$ frequencies of these fundamental modes and some combinational modes between them. Although curvature effects for the force constants are taken into account in our model, the approximation begins to break down for nanotube diameters smaller than ~ 0.8 nm since the long-range force constants are significantly affected by the curvature of the nanotube. For lower-frequency modes, the influence of the curvature effects is relatively small.

Based on the frequencies of the calculated phonon modes in Fig. 3, we can now discuss the origins of the observed fourteen peaks. First, we attribute Peak #1 at $\sim 85\text{ cm}^{-1}$ to the E_2 (iTA-like) mode, whose predicted value is 76 cm^{-1} . Given the uncertainty of $\pm 50\text{ cm}^{-1}$ in the theoretically calculated values, which depends on the choice of force constants,³³ this is reasonable agreement. We also speculatively assign the weak and broader peak at $\sim 175\text{ cm}^{-1}$ (Peak Y) to the E_1 (LA-like) mode, whose calculated value is 213 cm^{-1} . In addition, the weak peak near 280 cm^{-1} (Peak Z), just below the RBM, could be due to a combinational mode between the 1st E_2 (iTA-like, 76 cm^{-1}) and the 2nd E_1 (LA-like, 213 cm^{-1}) modes; such a combinational mode between acoustic phonons has been seen in a graphite whisker³⁶ and multi-wall carbon nanotubes³⁷ and is believed to arise through a double-resonance process.³⁸

As seen in Fig. 2e, four pronounced IFM peaks (Peaks #6-#9) appear in pairs, symmetrically separated from the center frequency at 883 cm^{-1} . We interpret this central frequency as that of the oTO mode, which is predicted to have a frequency of 884 cm^{-1} , again in excellent agreement. Then the two pairs of IFM peaks can be understood as the sum (+) and difference (−) frequencies, respectively, of the oTO mode and i) the 1st E_2 mode (iTA-like, 76 cm^{-1}) and ii) the 2nd E_1 mode (LA-like, 213 cm^{-1}). In addition, the weaker IFM peaks at 623 cm^{-1} (Peak #5) and 1145 cm^{-1} (Peak #10) can also be the sum and difference, respectively, of the oTO mode and the sum of i) and ii) (three phonon combinations) although it is also likely that Peak #5 is the RBM overtone as previously observed in Raman.³⁰ Furthermore, there are two other IFM peaks, that is, Peaks #3 and #4. Peak #3 at 487 cm^{-1} can be assigned to a combinational mode between the RBM (294 cm^{-1}) and the 2nd E_1 mode (LA-like, 213 cm^{-1}). Peak #4 at 574 cm^{-1} can be assigned to a combination of three different symmetry modes, that is, the RBM (A_1 , 294 cm^{-1}), the 2nd E_1 mode (LA-like, 213 cm^{-1}), and the 1st E_2 mode (iTA-like, 76 cm^{-1}).

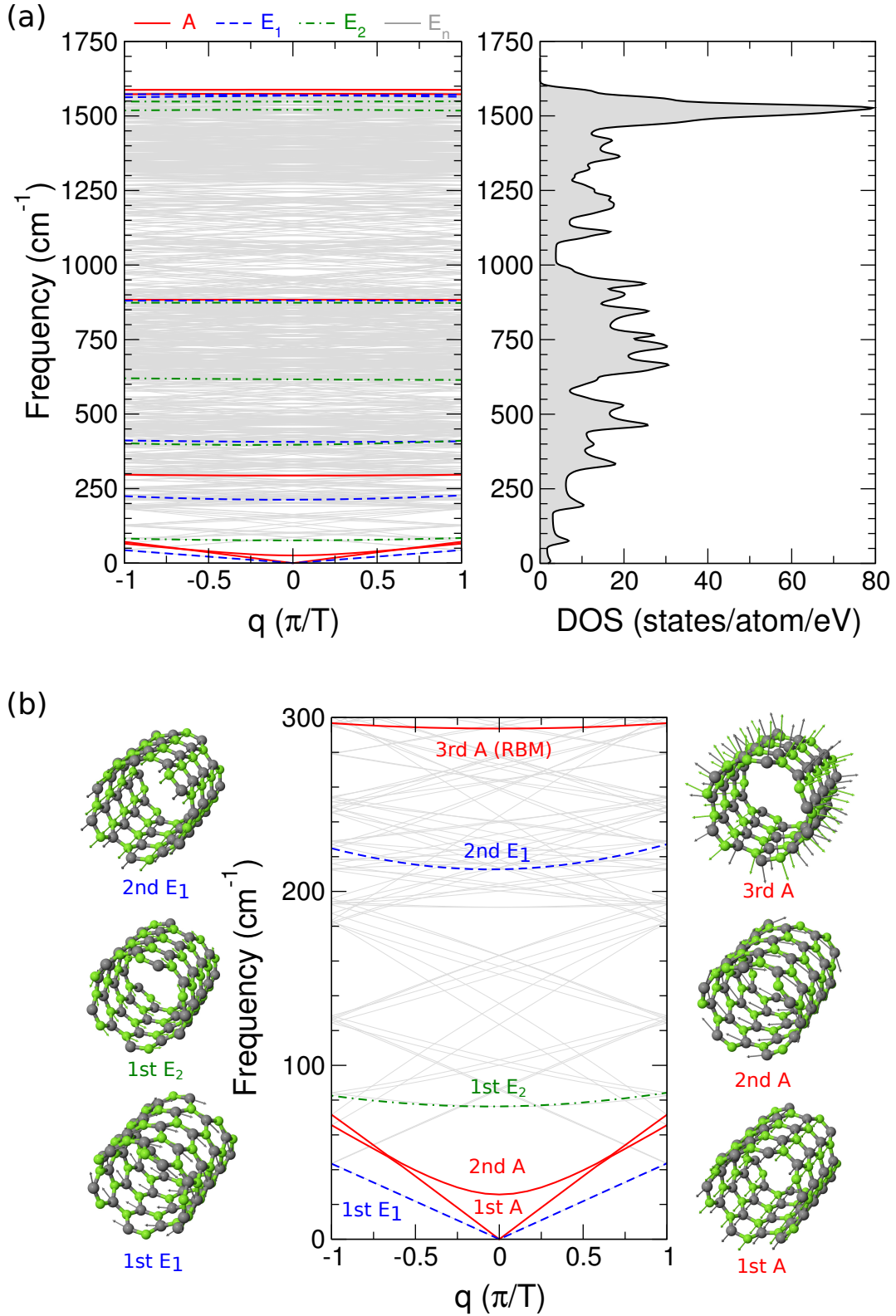


FIG. 3: (a) Calculated phonon dispersion curves (left) and corresponding density of states (right) for possible phonon modes (A, E_1 , E_2) for the (6,5) carbon nanotube, obtained by the extended tight-binding model. Each symmetry mode is distinct from others by its color and has all the same six-fold phonon branches from the bottom. (b) Enlarged dispersion curve in the low-frequency region with pictures to display the corresponding eigenvector motions of carbon atoms.

TABLE I: Experimentally measured and theoretically predicted frequencies of various coherent phonon (CP) modes for (6,5) single-wall carbon nanotubes, including both fundamental and combinational modes, together with assignments and CW Raman values. Peak Number refers to the labels indicated for the observed CP peaks in Fig. 2c. The values in the Theory column were calculated through the extended tight-binding model.³⁵

Peak Number	CP (cm ⁻¹)	Assignment	Raman (cm ⁻¹)	Theory (cm ⁻¹)
#1	86±3	1 st E ₂ (iTA)		76
		2 nd E ₁ (LA)		213
#2	309±2	3 rd A (RBM)	309	294
		2 nd E ₂ (LA-like)		397
		3 rd E ₁	399	407
		3 rd E ₁	423	407
#3	487±4	RBM + 2 nd E ₁		507
#4	574±4	1 st E ₂ + 2 nd E ₁ + RBM		582
#5	623±9	RBM overtone or oTO - 1 st E ₂ - 2 nd E ₁	621	588 (595)
		3 rd E ₂		616
			668	
			692	
#6	718±1	oTO - 2 nd E ₁	710	671
#7	807±5	oTO - 1 st E ₂		807
			837	
			853	
	883±12	4 th A (oTO)		884
		4 th E ₂		874
		4 th E ₁		881
			908	
#8	970±6	oTO + 1 st E ₂		960
			1027	
#9	1054±3	oTO + 2 nd E ₁	1057	1096
#10	1145±6	oTO + 1 st E ₂ + 2 nd E ₁		1173
		D	1312	1338
		5 th E ₂		1521
		5 th E ₁		1568
		5 th A (iTO or G ⁻)	1528	1575
#11	1588±4	6 th A (LO or G ⁺)	1589	1588
		6 th E ₁		1570
		6 th E ₂		1548
#12	1764±4	LO + 2 nd E ₁		1801
#13	1866±4	LO + 1 st E ₂ + 2 nd E ₁		1877
#14	2591±4	2D (or G')		2618

Previous Raman measurements on chirality-mixed SWCNT samples detected some IFMs in the 600-1100 cm⁻¹ frequency range excited in the E₃₃/E₄₄ region²⁶ as well as in the 370-480 cm⁻¹ frequency range excited in the E₁₁/E₂₂ region.^{29,30} Fantini *et al.* observed only two peaks associated with the oTO mode combined with acoustic phonon modes.²⁶ The so-called 'step-wise' dispersive behaviors were observed in these studies because the IFMs have a strong chirality- and diameter-dependence, which jumps when the excitation photon energy goes from one $2n + m$ family to another. Kilina and co-workers³⁹ suggested some connection be-

tween the resonances for these particular IFMs and cross-polarized transitions, which may be reasonable with the E-symmetry character of these modes. However, in all these previous studies on chirality-mixed ensembles, the analysis and ultimate (n,m) assignment of specific IFMs were model-dependent, and thus, the determined IFM frequencies depended on the assumption that the (n,m) assignments were correct. On the contrary, the present work on IFM coherent phonons represents a single (n,m) probe of IFM behavior, providing model-independent frequencies.

Lastly, it is interesting to note some distinct differences between Raman and CP spectra. First, Raman observed a clear D-peak at ~ 1312 cm⁻¹ (see 1f) whereas it was absent in the CP spectra (see Fig. 2c). Second, a clear G⁻ peak was observed at ~ 1528 cm⁻¹ in Raman (see Fig. 1f) whereas it was not clearly observed in CP (see Fig. 2c). We are currently modeling the CP generation and detection processes for various phonon modes, including the D and G⁻ modes, to compare their expected intensities with the experimental observations. Furthermore, in Raman we see an IFM at ~ 399 cm⁻¹, ~ 420 cm⁻¹, ~ 668 cm⁻¹, ~ 692 cm⁻¹, ~ 837 cm⁻¹, ~ 853 cm⁻¹, ~ 908 cm⁻¹, and ~ 1027 cm⁻¹ (see Figs. 1d-e and Table I), which do not agree with any of the clearly observed CP peaks. It should be noted that any short-lived phonon mode cannot be detected in CP spectroscopy because they are significantly affected by the fast and strong electronic pump-probe signal (especially important in SWCNTs). In our CP analysis, we did not use any data before ~ 125 fs, and therefore, if the peak width exceeds ~ 80 cm⁻¹, the peak is not recorded. This is a possible explanation as to why CP does not show the broad peaks at 853 cm⁻¹ and 908 cm⁻¹ observed in Raman. In addition, the phonon generation mechanism by photo-excited carriers (exciton-phonon interaction in the case of SWCNTs) should be common for Raman spectroscopy and ultrafast pump-probe spectroscopy. However, in the case of Raman spectroscopy, we measure the photon energy of the scattered light while in the case of pump-probe spectroscopy we measure the reflectance or transmittance of the probe beam. The optical response of the material to the probe beam in the presence of the phonons may not always be the same as that for the Raman spectra. The modifications of the probe reflectance and transmittance should depend on phonon vibration amplitudes and directions. A further investigation is under way.

V. CONCLUSION

In conclusion, by combining the excellent signal-to-noise ratio and spectral resolution of coherent phonon spectroscopy with a highly-enriched, single-chirality (6,5) single-wall carbon nanotube sample, we have detected previously unobserved vibrational modes. The combination of a modern SWCNT separation technique with ad-

vanced ultrafast optical spectroscopy allowed direct observations of several phonon branches of A , E_1 , and E_2 symmetries and their combinations. We demonstrated that there is strong coupling between different phonon modes over a wide frequency range. By presenting a detailed compendium of phonons for single-chirality single-wall carbon nanotubes, this work serves as a reference with which to refine our understanding of the dynamics and interactions of one-dimensional phonons and electrons and as a testbed for new theoretical models for more precise and accurate calculations. Furthermore, the present analysis shows that there is a clear discrepancy for some phonon modes between Raman and pump probe measurements, whose reasons remain to be explained.

Acknowledgements

This work was supported in part by the National Research Foundation of Korea (NRF) grant funded by the Korea government (MEST) (2013R1A1A2006659, 2010-022691). TJ acknowledges the support by the Na-

tional Research Foundation of Korea (NRF) grant funded by the Korea government (MSIP) (2007-0056330) and the Global Research Laboratory Program (2009-00439). JK acknowledges support by the Department of Energy (through Grant No. DE-FG02-06ER46308), the National Science Foundation (through Grants No. OISE-0968405), and the Robert A. Welch Foundation (through Grant No. C-1509). GDS and CJS acknowledge support from the National Science Foundation through grants OISE-0968405 and DMR-1105437. HL acknowledges support by the “100 talents project” of CAS and the recruitment program of global youth experts. HK acknowledges support by JSPS KAKENHI Grant Number 25220602. RS acknowledges support by KAKENHI (Nos. 25286005 and 25107005). ARTN acknowledges the support by the JSPS Research Fellowship for Young Scientists (201303921). Raman spectra were acquired at the Center for Integrated Nanotechnology, a U.S. Department of Energy, Office of Basic Energy Sciences user facility. EHH, HT, and SKD acknowledge partial support from the LANL LDRD program.

-
- * kono@rice.edu; corresponding author.
 † thjoo@postech.ac.kr; corresponding author.
 ‡ Present address: Sungkyunkwan University, Jangan-gu, Suwon, Republic of Korea
- ¹ M. Zheng, A. Jagota, M. S. Strano, A. P. Santos, P. Barone, S. G. Chou, B. A. Diner, M. S. Dresselhaus, R. S. McLean, G. B. Onoa, et al., *Science* **302**, 1545 (2003).
 - ² M. Zheng, A. Jagota, E. D. Semke, B. A. Diner, R. S. McLean, S. R. Lustig, R. E. Richardson, and N. G. Tassi, *Nat. Mat.* **2**, 338 (2003).
 - ³ M. S. Arnold, S. I. Stupp, and M. C. Hersam, *Nano Lett.* **5**, 713 (2005).
 - ⁴ M. S. Arnold, A. A. Green, J. F. Hulvat, S. I. Stupp, and M. C. Hersam, *Nat. Nanotechnol.* **1**, 60 (2006).
 - ⁵ S. Ghosh, S. M. Bachilo, and R. B. Weisman, *Nat. Nanotechnol.* **5**, 443 (2010).
 - ⁶ H. Liu, D. Nishide, T. Tanaka, and H. Kataura, *Nat. Commun.* **2**, 309 (2011).
 - ⁷ X. Tu, A. R. Hight Walker, C. Y. Khripin, and M. Zheng, *J. Am. Chem. Soc.* **133**, 12998 (2011).
 - ⁸ C. Y. Khripin, J. A. Fagan, and M. Zheng, *J. Am. Chem. Soc.* **135**, 6822 (2013).
 - ⁹ E. H. Haroz, W. D. Rice, B. Y. Lu, S. Ghosh, R. H. Hauge, R. B. Weisman, S. K. Doorn, and J. Kono, *ACS Nano* **4**, 1955 (2010).
 - ¹⁰ J. G. Duque, H. Chen, A. K. Swan, A. P. Shreve, S. Kilina, S. Tretiak, X. Tu, M. Zheng, and S. K. Doorn, *ACS Nano* **5**, 5233 (2011).
 - ¹¹ E. H. Haroz, J. G. Duque, W. D. Rice, C. G. Densmore, J. Kono, and S. K. Doorn, *Phys. Rev. B* **84**, 121403(R) (2011).
 - ¹² E. H. Haroz, J. G. Duque, B. Y. Lu, P. Nikolaev, S. Arepalli, R. H. Hauge, S. K. Doorn, and J. Kono, *J. Am. Chem. Soc.* **134**, 4461 (2012).
 - ¹³ E. H. Haroz, J. G. Duque, X. Tu, M. Zheng, A. R. H. Walker, R. H. Hauge, S. K. Doorn, and J. Kono, *Nanoscale* **5**, 1411 (2013).
 - ¹⁴ Q. Zhang, E. H. Haroz, Z. Jin, L. Ren, X. Wang, R. S. Arvidson, A. Luttge, and J. Kono, *Nano Lett.* p. Article ASAP (2013).
 - ¹⁵ M. S. Dresselhaus, G. Dresselhaus, and P. Avouris, eds., *Carbon Nanotubes: Synthesis, Structure, Properties, and Applications*, no. 18 in Topics in Applied Physics (Springer, Berlin, 2001).
 - ¹⁶ P. Avouris, M. Freitag, and V. Perebeinos, *Nat. Photon.* **2**, 341 (2008).
 - ¹⁷ A. Jorio, G. Dresselhaus, and M. S. Dresselhaus, eds., *Carbon Nanotubes: Advanced Topics in the Synthesis, Structure, Properties and Applications* (Springer, Berlin, 2008).
 - ¹⁸ F. Leonard, *The Physics of Carbon Nanotube Devices* (William Andrew, Norwich, NY, 2009).
 - ¹⁹ S. Nanot, E. H. Haroz, J.-H. Kim, R. H. Hauge, and J. Kono, *Adv. Mater.* **24**, 4977 (2012).
 - ²⁰ R. Saito, G. Dresselhaus, and M. S. Dresselhaus, *Physical Properties of Carbon Nanotubes* (Imperial College Press, London, 1998).
 - ²¹ S. Reich, C. Thomsen, and J. Maultzsch, *Carbon Nanotubes: Basic Concepts and Physical Properties* (Wiley-VCH, Weinheim, 2004).
 - ²² M. S. Dresselhaus, A. Jorio, M. Hofmann, G. Dresselhaus, and R. Saito, *Nano Lett.* **10**, 751 (2010).
 - ²³ R. Saito, M. Hofmann, G. Dresselhaus, A. Jorio, and M. S. Dresselhaus, *Adv. Phys.* **60**, 413 (2011).
 - ²⁴ A. Jorio, M. S. Dresselhaus, R. Saito, and G. F. Dresselhaus, *Raman Spectroscopy in Graphene Related Systems* (Wiley-VCH, 2011).
 - ²⁵ A. C. Ferrari and D. M. Basko, *Nat. Nano.* **8**, 235 (2013).
 - ²⁶ C. Fantini, A. Jorio, M. Souza, R. Saito, G. G. Samsonidze, M. S. Dresselhaus, and M. A. Pimenta, *Phys. Rev. B* **72**, 085446 (2005).

- ²⁷ S. G. Chou, F. Plentz, J. Jiang, R. Saito, D. Nezich, H. B. Ribeiro, A. Jorio, M. A. Pimenta, G. G. Samsonidze, A. P. Santos, et al., *Phys. Rev. Lett.* **94**, 127402 (2005).
- ²⁸ H. Htoon, M. J. O'Connell, S. K. Doorn, and V. I. Klimov, *Phys. Rev. Lett.* **94**, 127403 (2005).
- ²⁹ Z. Luo, F. Papadimitrakopoulos, and S. K. Doorn, *Phys. Rev. B* **75**, 205438 (2007).
- ³⁰ Z. Luo, F. Papadimitrakopoulos, and S. K. Doorn, *Phys. Rev. B* **77**, 035421 (2008).
- ³¹ J.-H. Kim, A. R. T. Nugraha, L. G. Booshehri, E. H. Hároz, K. Sato, G. D. Sanders, K.-J. Yee, Y.-S. Lim, C. J. Stanton, R. Saito, et al., *Chem. Phys.* **413**, 55 (2013).
- ³² Y.-S. Lim, K.-J. Yee, J.-H. Kim, J. Shaver, E. H. Hároz, J. Kono, S. K. Doorn, R. H. Hauge, and R. E. Smalley, *Nano Lett.* **6**, 2696 (2006).
- ³³ Z. M. Li, V. N. Popov, and Z. K. Tang, *Solid State Commun.* **130**, 657 (2004).
- ³⁴ J. Maultzsch, S. Reich, C. Thomsen, H. Requardt, and P. Ordejón, *Phys. Rev. Lett.* **92**, 075501 (2004).
- ³⁵ J. Jiang, R. Saito, G. G. Samsonidze, S. G. Chou, A. Jorio, G. Dresselhaus, and M. S. Dresselhaus, *Phys. Rev. B* **72**, 235408 (2005).
- ³⁶ P. Tan, C. Hu, J. Dong, W. Shen, and B. Zhang, *Phys. Rev. B* **64**, 214301 (2001).
- ³⁷ P. Tan, L. An, L. Liu, Z. Guo, R. Czerw, D. L. Carroll, P. M. Ajayan, N. Zhang, and H. Guo, *Phys. Rev. B* **66**, 245410 (2002).
- ³⁸ R. Saito, A. Jorio, A. G. Souza Filho, G. Dresselhaus, M. S. Dresselhaus, and M. A. Pimenta, *Phys. Rev. Lett.* **88**, 027401 (2001).
- ³⁹ S. Kilina, S. Tretiak, S. K. Doorn, Z. Luo, F. Papadimitrakopoulos, A. Piryatinski, A. Saxena, and A. R. Bishop, *Proc. Nat. Aca. Sci.* **105**, 6797 (2008).